Kalpa Publications in Computing

Volume 22, 2025, Pages 390–399

Proceedings of The Sixth International Conference on Civil and Building Engineering Informatics

3D Scene Understanding for Highway Tunnel Construction: Challenges and Baseline Analysis

Li-zhuang Cui[1], Lei Kou[2], Hanming Zhang[3], Feng Guo[4], and Jian Liu[5, *]

1) Ph.D. Candidate, School of QILU Transportation, Shandong University, Jinan, China. Email: cvlizhuang@163.com
2) Ph.D., School of QILU Transportation, Shandong University, Jinan, China. Email: lei.kou@sdu.edu.cn
3) Ph.D., School of QILU Transportation, Shandong University, Jinan, China. Email: hmzhang619@sdu.edu.cn
4) Ph.D., Assoc. Prof. School of QILU Transportation, Shandong University, Jinan, China. Email: fengg@sdu.edu.cn
5) Ph.D., Prof., School of QILU Transportation, Shandong University, Jinan, China. Email: liujianshanda@gmail.com

Abstract: 3D scene understanding is revolutionising tunnel engineering. However, deep learning algorithms are data-hungry, which means the application of scene understanding on tunnel engineering requires a customized point cloud dataset in the construction field. In this paper, we introduce a new point cloud dataset called HTunnel-HLS, specifically designed for construction highway tunnel environment. HTunnel-HLS aims to establish a new database for developing semantic segmentation, and importantly, construction highway tunnel scene. Besides, the dataset provides both point-level semantic labelling along with a large range of types of semantic instance labels categorized into support structures, mechanical facilities, and others. Data have been acquired by the Hand Laser Scanning (HLS) system Hovermap and contains 28 scenes, over 1.58 billion 3D points, correspond to a 9 km long tunnel section. This paper also provides the performance of several representative baseline methods. The impact of scale on model performance is analyzed from the perspective of grid size, and outlines potential future works and challenges for fully exploiting this dataset.

Keywords: LiDAR, 3D Point cloud, Semantic segmentation, Tunnel construction.

1. INTRODUCTION

Construction safety and quality are key performance indicators for mechanized tunneling, especially in light of the rising promise of unmanned construction (Rachmawati, 2022). In order to ensure safety, long term stability and quality control in modern tunneling operations, the acquisition of geotechnical information about encountered rock conditions (Yi, 2023), detailed installed support (Wang, 2023) and rate of advancement information is required. Data collection as the tunnel progresses must make use of fast and effective technology in order to surmount operational constraints (Fekete, 2010). And it is important to inspect and evaluate the structures during construction (Cui, 2024; Zhang,2025).

Point clouds, as the most direct representation of real-world 3D digitalization, have been applied to tunnel construction and management (Zhao, 2023). Point clouds acquired by laser scanning

are valuable digital assets for highway tunnels, which can be used for tunnel profile control (Kim, 2019), joint surface analysis (Xu, 2022), lining quality assessment (Lato, 2014), tunnel deformation monitoring (Deng, 2024), and 3D model reconstruction (Duan, 2021). However, A prerequisite for automatic extraction of present-day kinds of tasks is the identification of individual structures from the background scene. Conventional, heuristic algorithms suffer from several drawbacks in efficiency and generalization (Chi, 2023; Xie, 2020).

The emergence of deep learning technology has already shown considerable promise for improving the efficiency and accuracy of tunnel management. However, most recent researches have explored the application of 3D deep learning networks to the point cloud segmentation task of shield tunneling (Lin, 2024; Xie, 2023; Xie, 2017) rather than drill-and-blast highway tunnel. Empirically, data collection at drill-and-blast tunnel construction sites is more challenging than conventional scanning operations. Although emerging datasets for semantic segmentation have been proposed (A, 2013; Munoz, 2009; Ye, 2020; Zolanvari, 2019; Tong, 2020), few of them provide point-wise instance annotation for construction highway tunnel scene on a large scale. At the drill-and-blast tunnel construction site, the structural complexity of elongated spaces and the procedural continuity of dynamic construction pose significant challenges to the acquisition and annotation of 3D laser point clouds. This is why it is difficult to find annotated point cloud datasets related to tunnel engineering in popular open-source datasets, especially for construction tunnels. In contrast, there is a distinct lack of annotated datasets for highway tunnel point clouds which presents a significant obstacle for 3D deep learning segmentation. Thus, specialized datasets and their corresponding benchmarks are urgently required for the development of 3D deep learning for highway tunnel point clouds.

To that end, this paper introduces a new and richly annotated tunnel point cloud dataset, 'HTunnel-HLS', to enable automated semantic segmentation using 3D deep learning. Data experiments are presented to explore the influences of grid size in data preprocessing on the 3D deep learning model performance. This study also provides corresponding benchmarks by applying typical 3D deep learning networks to the SDU-Tunnel3D dataset. Data will be acquired and processed soon.

2. NEW DATASET: HTUNNEL-HLS

2.1 Data acquisition

This study is based on a highway tunnel under construction. The highway tunnel is a three-lane road tunnel with a triple-circle curved wall lining structure, where the New Austrian Tunneling Method (NATM) is adopted. Considering factors such as tunnel structure, face stability, and geological conditions, this tunnel is constructed by the drill-and-blast method, which is specifically constructed by the bench cut method. The bench cut method involves excavating the designed profile in two stages: upper and lower sections, with the upper section excavated first followed by the lower section.

Table 1. The key technical specifications of the HLS.

Indicator item	Parameter	Indicator item	Parameter
Scan distance	0.4m~100m	LiDAR accuracy	+/- 30mm
Mapping accuracy	+/- 15mm	Angular field of view	360°×360°
Maximum data capture travelling speed	2 m/s	Data acquisition speed	Up to 3×10^5 points/sec

Observations at the tunnel construction site, Figure 1 (a), reveal narrow and confined working spaces, with tight operations of machinery and vehicles. The acquisition has been carried out by the handheld laser scanners (HLS) named Hovermap, and produced by Emesent, as shown in Figure 1 (b). Table 1 summarizes the key technical specifications of the device. The procedure used to collect our LiDAR point cloud dataset is similar to previously published work (Cui, 2023). In addition to the tunnel structural elements, each point cloud also includes cables, pipes, loose rocks, construction vehicles, and

other non-structural elements, Figure 1 (c). Hence, all possible elements and noise that may affect the point cloud segmentation are considered in the present dataset. The point clouds in HTunnel-HLS are acquired by HLS and have similar point density distributions, which differs from the feature that point clouds acquired using TLS decreases with distance to the scanner.

Figure 1. (a) The tunnel construction site; (b) Tunnel 3D point cloud data is being collected using HLS on the site ; (c) Complex point cloud data of tunnel construction site (Cui, 2023).

2.2 Data annotation

To achieve rigorous model training and evaluation, the data annotation needs to be comprehensive, consistent, and accurate for the specified labels. Instead of pixel-wise or voxel-wise annotation, every single point in HTunnel-HLS is labelled individually. This exhaustive manual annotation of the ground truth dataset avoids any biases introduced by particular segmentation algorithms.

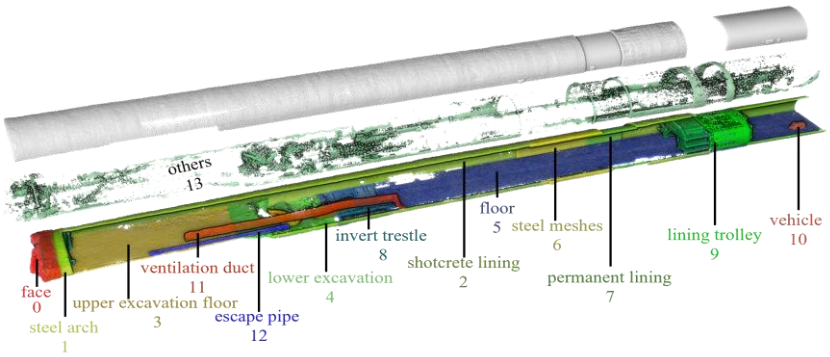

Figure 2. A representative example of labels and classes on a 3D point cloud.

In general, we categorize instances in construction tunnels into 3 classes: support structures, mechanical facilities, and others, with a total of 14 semantic labels. In the class “others” include noise points, water and electrical pipelines, ducts, loose rocks, personnel, debris, trailing shadows, etc. As objects from real-world scans are often cluttered with background and/or are partial due to occlusions. To prevent confusion, Fig. 2 illustrates a representative example of labels and classes on a 3D point cloud. A color represents a category and corresponds to a semantic label. It is important to note that by default, if an unknown class is encountered, it will be treated as 'others'.

Our annotation process does not entail labeling every point in the point cloud. Instead, we employ 3D clipping to segment all point clouds into different instances and assign a category to each segmented object, which are then individually saved in separate files. All point cloud annotations are hand-labeled by professional assessors and undergo manual cross-checking. We manually scrutinize

each object, rectify inconsistent labels, and discard ambiguous, low-quality reconstruction, unlabeled, sparsely populated, and insufficient instances to form a category for training. This ensures the consistency and high quality of the annotation work. The point clouds are segmented manually using CloudCompare software. Unlike the cluttered spatial relationships of instances, the spatial distribution of instances inside tunnels is traceable.

2.3 Description of the dataset

The resulting HTunnel-HLS dataset is analysed to provide quantitative insights into its key characteristics. The dataset consists of 28 tunnel segments categorized into 14 classes, as a result, 586 objects are annotated. This extensive scale provides novel avenues for training data-intensive algorithms. The point cloud proportion of each class is presented in Fig. 3, showing that the HTunnel-HLS dataset is 'class-imbalanced' where label 'ShotcreteLining' accounts for the greatest proportion of the point clouds. While mechanical facilities e.g., escape pipe, invert trestle, and vehicle have fewer points, which is consistent with the situation of the construction sites. In addition, point clouds captured by the Hovermap scanner include not only x, y, z Cartesian coordinates but also real-world dimensions such as intensity, GPS time, return number, range, and ring etc. In order to better examine the performance and generalization of deep learning algorithms, only the original x, y, z Cartesian coordinates of each point is retained in the dataset to ensure data consistency and fair comparison. From Fig. 2, it can be observed that there is critically shape similarity between the shotcrete lining and permanent lining, as well similarity in the scale. Comparing the results for upper excavation floor and floor, shape similarity is also observed. This similarity highlights the difficulty in identifying individual segments using 3D deep learning. The training set and test set are split artificially 23:5 (respectively).

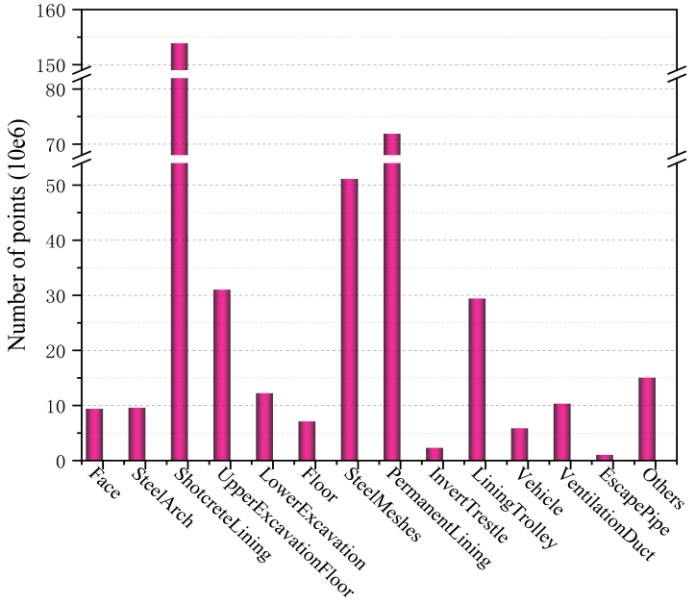

Figure 3. The point cloud proportion of each class.

3. EXPERIMENTS AND DISCUSSION

3.1 Baseline approaches for semantic segmentation

We only selected algorithms that have published results and available codes, and three popular point-based deep learning models for semantic segmentation were tested on the proposed dataset as

baseline approaches:

DGCNN (Wang, 2018) suggests that local geometric features are important to 3D recognition tasks, and the model constructs graphs to extract local geometric features from local neighborhoods, and applies EdgeConv as a convolution-like operation. EdgeConv is isotropic about input features with convolutional operations on graph nodes and their edges.

RandLA-Net (Hu, 2020) utilizes random point sampling and introduces a local feature aggregation module to achieve rapid processing of large-scale point clouds while effectively preserving geometric details.

Point Transformer V3 (Wu, 2024), a stride towards overcoming the traditional trade-offs between accuracy and efficiency in point cloud processing, redefines the framework of Point Transformer. PTv3 reverts to utilizing dot-product attention. By prioritizing efficiency over the accuracy of less impactful mechanisms, PT v3 harness the power of scale, leading to enhanced performance. Simply put, the model becomes stronger by being made simpler and faster.

3.2 Evaluation metrics and configurations

For semantic segmentation, OA (overall accuracy; Equation (1)), IoU (interaction over union; Equation (2)) and mIoU (mean interaction over union; Equation (3)) are employed to evaluate model performance. In particular, mIoU presents the most reasonable evaluation for class-imbalanced datasets and is thus adopted as the priority metric.

$$OA = \frac{\sum TP_n}{Total\ number\ of\ points} \quad \text{Equation (1)}$$

$$IoU_n = \frac{TP_n}{TP_n + FP_n + FN_n} \quad \text{Equation (2)}$$

$$mIoU = \frac{\sum IoU_n}{N} \quad \text{Equation (3)}$$

where N is the total number of labels; n is the nth label in N; TP, FP and FN represent numbers of points of true positives, false positives, and false negatives of the predictions, respectively. OA and mIoU evaluate the overall quality of semantic segmentation; and IoU of each class measures the performance of each class.

In this study, the results were for baseline illustration purpose only, and better results could be potentially achieved with further tuning. Batch sizes were adjusted accordingly, and the remaining hyperparameters within the original model were not modified. The network structures and parameter settings of these algorithms may not be directly comparable, and parameter tuning does not guarantee the fairness of comparison. In this study, the results are for baseline illustration purpose only, and better results could be potentially achieved with further tuning. All models were trained and tested on a NVIDIA RTX 2080Ti with 11G of RAM. And batch sizes were adjusted accordingly.

3.3 Performance of baseline approaches

The results for semantic segmentation baseline approaches using HTunnel-HLS are shown in Table 2. PT V3 is on the top spot of HTunnel-HLS benchmark at the moment, and it achieved the highest OA, mACC, and mIoU among the tested baseline algorithms. DGCNN performed the worst in terms of OA, mACC, and mIoU in our dataset. And PT V3 has a significant performance improvement in the segmentation of these 14 types of objects. Since DGCNN uses KNN for construction of graphs to capture local features, it may not perform well in this dataset with varying point density and Class Imbalance Problem. The IoU of all three models is relatively low in steel arch class. It is worth

mentioning that RandLA-Net is the first to complete the entire training process of 100 epochs, PT V3 is the second, and DGCNN takes the longest time.

Table 2. Semantic segmentation results of different methods (%).

Methods	OA	mIoU	mACC	0	1	2	3	4	5	6	7	8	9	10	11	12	13
DGCNN	0.8221	0.5867	0.7066	0.3637	0.3207	0.7193	0.7965	0.5725	0.8788	0.7652	0.5724	0.5169	0.7601	0.6183	0.6699	0.3692	0.2897
RandLA-Net	0.8397	0.7154	0.8520	0.5709	0.3603	0.7160	0.5785	0.6664	0.8311	0.9201	0.7157	0.7985	0.9324	0.7857	0.8635	0.8771	0.3990
PT V3	0.9700	0.9099	0.9481	0.9403	0.7615	0.9651	0.9184	0.9089	0.9586	0.9558	0.9852	0.9501	0.9582	0.8697	0.9789	0.9534	0.6345

4. DISCUSSION

As mentioned in Point Transformer V3, model performance is more profoundly influenced by scale than by complex design intricacies. The scale of the tunnel point cloud dataset constructed in this paper is significantly larger than that of indoor scenes and also exceeds that of common road scenes in terms of both the number and density of points. It is both common and necessary to the input point clouds preprocessing before deep learning training and evaluation to improve computational efficiency, whilst also minimizing the effect on accuracy. In general, the density of the input point cloud is reduced through sampling, and memory consumption is reduced. Appropriate sampling resolution is very important for the test results. For public data set S3DIS (indoor scene) (Armeni, 2016), the sampling resolution is 0.04 by default, and for semantic3d (Hackel, 2017) and SemanticKITTI (outdoor street scene) (Behley, 2019), the sampling resolution is 0.06 by default. When the input size is kept constant, the lower input sampling resolution represents a larger receptive field, higher performance and faster training efficiency. Of course, the corresponding price to be paid is the possible loss of local information. Therefore, it is necessary to determine the appropriate grid size for the newly established tunnel scene dataset.

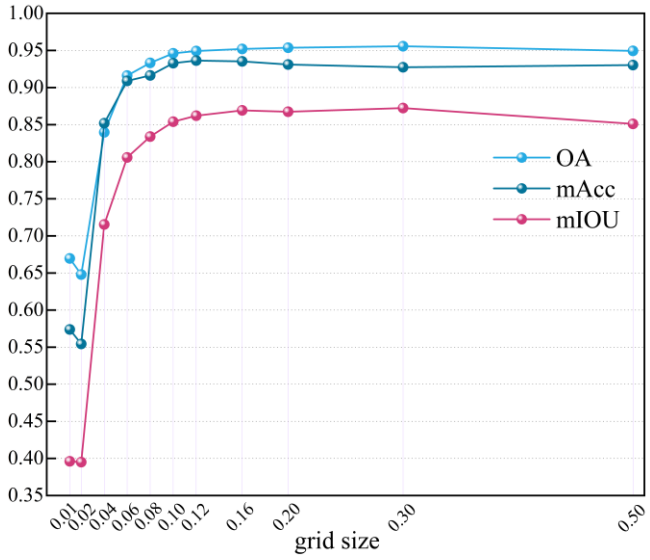

Figure 4. The performance curve obtained after data preprocessing with different grid sizes.

Table 3. Semantic segmentation results of different grid size.

Models	Grid size	mIOU	0	1	2	3	4	5	6	7	8	9	10	11	12	13

G1	0.01	0.3961	0.1612	0.2823	0.5273	0.3370	0.3567	0.5921	0.8634	0.5117	0.3281	0.7192	0.0243	0.6221	0.0000	0.2202
G2	0.02	0.3951	0.2791	0.1736	0.5288	0.1891	0.2232	0.5826	0.9005	0.4294	0.5607	0.7213	0.0227	0.7017	0.0000	0.2190
G3	0.04	0.7154	0.5709	0.3603	0.7160	0.5785	0.6664	0.8311	0.9201	0.7157	0.7985	0.9324	0.7857	0.8635	0.8771	0.3990
G4	0.06	0.8058	0.6808	0.4534	0.8758	0.8061	0.7400	0.8973	0.9380	0.8967	0.8796	0.9536	0.9284	0.8854	0.8883	0.4580
G5	0.08	0.8339	0.7234	0.5557	0.9175	0.8215	0.8010	0.8995	0.9355	0.9252	0.8853	0.9630	0.9143	0.9280	0.9056	0.4988
G6	0.10	0.8540	0.7490	0.5819	0.9395	0.8955	0.8836	0.9177	0.9340	0.9606	0.8887	0.9655	0.8861	0.9171	0.9297	0.5076
G7	0.12	0.8621	0.7699	0.6179	0.9449	0.9002	0.8811	0.9225	0.9274	0.9658	0.9109	0.9651	0.8698	0.9431	0.9330	0.5173
G8	0.16	0.8693	0.8443	0.5440	0.9333	0.9194	0.9033	0.9256	0.9386	0.9735	0.9262	0.9796	0.9167	0.9390	0.8920	0.5350
G9	0.20	0.8674	0.8051	0.6090	0.9410	0.9128	0.8899	0.9366	0.9395	0.9708	0.9011	0.9755	0.9099	0.9439	0.8704	0.5377
G10	0.30	0.8724	0.8519	0.6079	0.9511	0.9201	0.8996	0.9355	0.9375	0.9726	0.8954	0.9259	0.8842	0.9599	0.9378	0.5347
G11	0.50	0.8510	0.8001	0.6076	0.9454	0.9074	0.8385	0.9147	0.9368	0.9646	0.8651	0.9637	0.8815	0.9373	0.8538	0.4972

Preprocess the raw point cloud and eleven models are trained using different input sizes, as listed in Table 3. RandLA-Net (Hu, 2020) containing a random sampling module is adopted here considering the remarkably computation and memory efficiency. Although RandLA-Net is no longer limited to 1m×1m blocks compared with pointnet++ (Qi, 2017), it can effectively learn the overall geometric structure of objects. However, for a brand-new semantic segmentation scenario, it is crucial to know how to set up the hyperparameters. The results show that when the grid size exceeds 0.12, there is a plateau in model performance (Figure 4). The mIoU of Model G6 reaches 86.21%. In the process of random sampling, number of input points, i.e., the number of nearest neighbors of the query point, is set to 40960, so a larger grid size means a larger receptive field, as shown in Figure 5. As a result, this means that the model is able to learn the overall geometry of the object more efficiently during training. As a larger range of point clouds are added to the training dataset, there is a notable increase in both OA and, in particular, mIoU. However, it is reasonable to expect a degradation of the model's performance when the grid size is too large, such as over 0.3, as this will discard the key features. The point cloud is downsampled with a four-fold decimation ratio.

During the training process, a loss function is typically used to intuitively show the trend of the difference between the model's predictions and the ground truth as the number of iterations increases. Under the same learning rate and batch size settings, the loss curves of models with different grid sizes during the training process are plotted as shown in Figure 6. Ideally, the loss curve should show a gradual decline and tend to stabilize. This indicates that as training progresses, the model's performance on the training set continues to improve. It can be observed that from G7 onward, this trend is evident. However, when the grid size is less than 0.12, the loss curve remains oscillatory and noisy throughout the training process, indicating that the loss function fails to converge. Conversely, when the grid size exceeds 0.12, the loss curve decreases rapidly in the early training stages and stabilizes, suggesting that the model converges quickly. This provides a parameter reference for achieving good performance in scenarios involving data such as tunnels. A visual comparison of semantic segmentation results of G7 (Grid size = 0.12 m) and ground truth is shown in Figure 7.

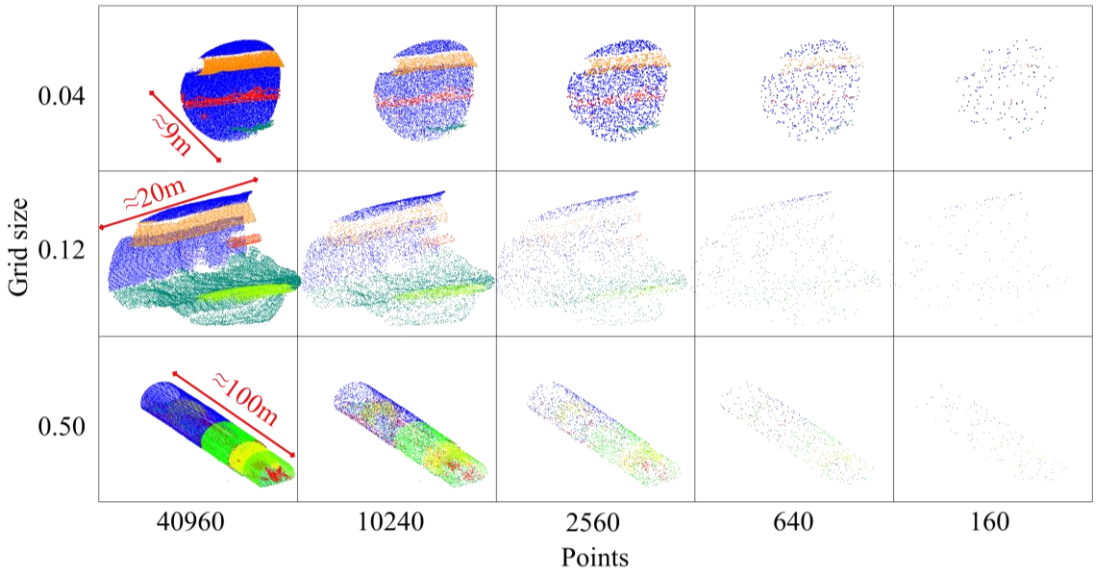

Figure 5. The area of points entered for each layer after setting different grid sizes.

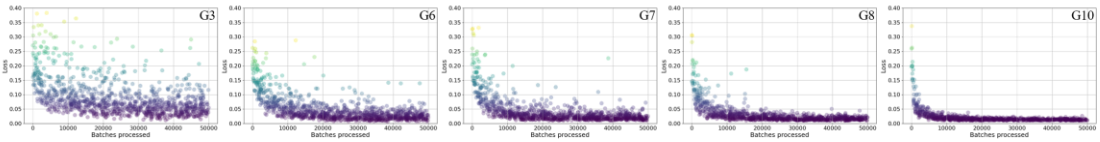

Figure 6. The loss curves of models with different grid sizes during the training process.

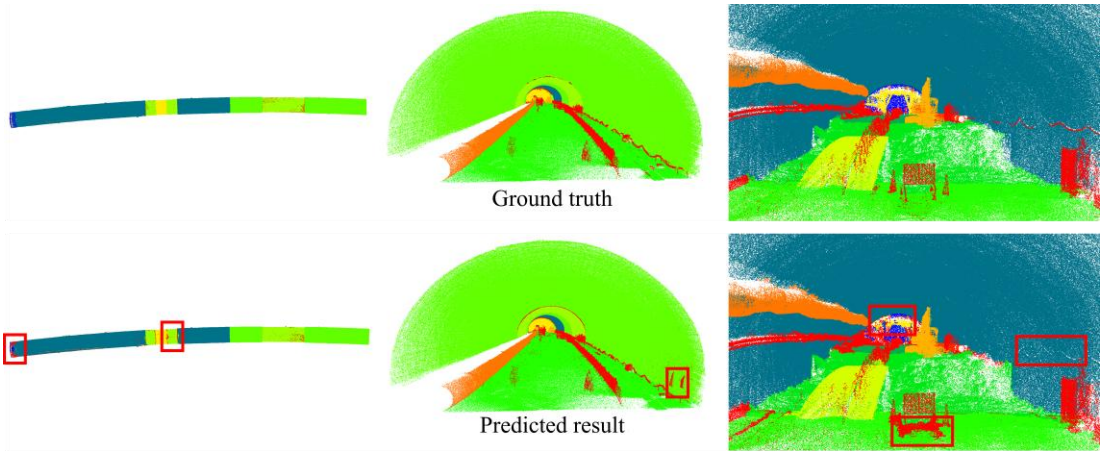

Figure 7. Visual comparison of results of semantic segmentation with different grid sizes.

4. CONCLUSIONS

We have presented a new 3D point cloud database manually annotated, specifically designed for construction highway tunnel environment. The dataset covers approximately 9 km of tunnel section with over 1.58 billion 3D points. Each 3D point has been classified into 14 categories, resulting in a list of (x, y, z) points. Three popular end-to-end point cloud semantic segmentation algorithms were tested as baselines for this dataset. We analyzed the impact of grid size on model performance and determined that a grid size of 0.12 is suitable for tunnel scenarios.

The intention of presenting this new tunnel point cloud dataset is to encourage developing creative deep learning models. This will promote the adoption and application of 3D point clouds in the tunnel engineering industry, thereby accelerating the digital transformation of traditional sectors. The labels of this new dataset will be improved and updated with feedback from the research community.

ACKNOWLEDGMENTS

This study is partially sponsored by Taishan Scholars Project, Grant Number: tstp20221153.

REFERENCES

A, M. H., A, M. A., and B, U. S. (2013). Change detection in urban areas by object-based analysis and on-the-fly comparison of multi-view als data. *ISPRS Journal of Photogrammetry and Remote Sensing*, 86(12), 52-64.

Armeni, I., Sener, O., Zamir, A., Jiang, H., Brilakis, I., and Fischer, M. (2016). 3d semantic parsing of large-scale indoor spaces. *IEEE Computer Society*.

Behley, J., Garbade, M., Milioto, A., Quenzel, J., Behnke, S., and Stachniss, C. (2020). SemanticKITTI: A Dataset for Semantic Scene Understanding of LiDAR Sequences. *2019 IEEE/CVF International Conference on Computer Vision (ICCV). IEEE.*

Chi, L., Yuhang, L. and Yuhua, C., (2023). A State-of-the-Practice Review of Three-Dimensional Laser Scanning Technology for Tunnel Distress Monitoring. *Journal of Performance of Constructed Facilities*, 37(2), pp.1-22.

Cui, L., Zhou, L., Xie, Q., Liu, J., Han, B. (2023). Direct generation of finite element mesh using 3D laser point cloud. *Structures.* V47 1579-1594.

Cui, L., Liu, J., Luo, H., Wang, J., Zhang, X., Lv, G. and Xie, Q., (2024). Deformation Measurement of Tunnel Shotcrete Liner Using the Multiepoch LiDAR Point Clouds. *Journal of Construction Engineering and Management*, 150(6), p.04024049.

Deng, H., Zhu, H. and Guo, J., (2024). Research on Deformation Monitoring of Roadway Surrounding Rock Based on Mobile 3D Laser Scanning Technology. *Academic Journal of Science and Technology*, 10(3), pp.155-162.

Duan, D.Y., Qiu, W.G., Cheng, Y.J., Zheng, Y.C. and Lu, F., (2021). Reconstruction of shield tunnel lining using point cloud. *Automation in Construction*, 130, p.103860.

Fekete, S., Diederichs, M. and Lato, M., (2010). Geotechnical and operational applications for 3-dimensional laser scanning in drill and blast tunnels. *Tunnelling and underground space technology*, 25(5), pp.614-628.

Hackel, T., Savinov, N., Ladicky, L., Wegner, J.D., Schindler, K. and Pollefeys, M., (2017). Semantic3d. net: A new large-scale point cloud classification benchmark. arxiv preprint arxiv:1704.03847.

Hu, Q., Yang, B., Xie, L., Rosa, S., and Markham, A. (2020). RandLA-Net: Efficient Semantic Segmentation of Large-Scale Point Clouds. *2020 IEEE/CVF Conference on Computer Vision and Pattern Recognition (CVPR). IEEE.*

Kim, Y. and Bruland, A., (2019). Analysis and evaluation of tunnel contour quality index. *Automation in Construction*, 99, pp.223-237.

Lato, M.J. and Diederichs, M.S., (2014). Mapping shotcrete thickness using LiDAR and photogrammetry data: Correcting for over-calculation due to rockmass convergence.

Tunnelling and Underground Space Technology, 41, pp.234-240.

Lin, W., Sheil, B., Zhang, P., Zhou, B., Wang, C., and Xie, X. (2024). Seg2tunnel: a hierarchical point cloud dataset and benchmarks for segmentation of segmental tunnel linings. *Tunnelling and Underground Space Technology incorporating Trenchless Technology Research*, 147.

Munoz, D., Bagnell, J. A., Vandapel, N., and Hebert, M. (2009). Contextual classification with functional max-margin markov networks. *IEEE*.

Qi, C. R., Su, H., Mo, K., and Guibas, L. J. (2017). Pointnet: deep learning on point sets for 3d classification and segmentation. *IEEE*.

Qi, C. R., Yi, L., Su, H., and Guibas, L. J. (2017). Pointnet++: deep hierarchical feature learning on point sets in a metric space.

Rachmawati, T.S.N. and Kim, S., (2022). Unmanned Aerial Vehicles (UAV) integration with digital technologies toward construction 4.0: A systematic literature review. *Sustainability*, 14(9), p.5708.

Thomas, H., Qi, C. R., Deschaud, J. E., Marcotegui, B., Goulette, F., and Guibas, L. (2020). KPConv: Flexible and Deformable Convolution for Point Clouds. *2019 IEEE/CVF International Conference on Computer Vision (ICCV). IEEE.*

Tong, G., Li, Y., Chen, D., Sun, Q., and Xiang, G. (2020). Cspc-dataset: new lidar point cloud dataset and benchmark for large-scale semantic segmentation. *IEEE Access*, PP (99), 1-1.

Wang Z, Hu M, Lai J, et al. (2023). Reliability analysis method for tunnel structural design: Brief review and relevant prospects. *Structures*, 55: 1894-1905.

Wang, Y., Sun, Y., Liu, Z., Sarma, S. E., Bronstein, M. M., and Solomon, J. M. (2018). Dynamic graph cnn for learning on point clouds. *ACM Transactions on Graphics, 38(5)*.

Wu, X., Jiang, L., Wang, P. S., Liu, Z., Liu, X., and Qiao, Y. (2024). Point Transformer V3: Simpler, Faster, Stronger. *2024 IEEE/CVF Conference on Computer Vision and Pattern Recognition*.

Xie, J., Huang, X., Zhang, Z., and Jin, G. (2023). Cohesive zone model-based analyses of localized leakage of segmentally lined tunnels. *Frontiers of structural and civil engineering*.

Xie, X., and Lu, X. (2017). Development of a 3d modeling algorithm for tunnel deformation monitoring based on terrestrial laser scanning. *Underground Space*, 2(1), 16-29.

Xie, Y., Tian, J., and Zhu, X. X. (2020). Linking points with labels in 3d: a review of point cloud semantic segmentation. *Geoscience and remote sensing* (4), 8.

Xu, Z.H., Yu, T.F., Lin, P., Wang, W.Y. and Shao, R.Q., (2022). Integrated geochemical, mineralogical, and microstructural identification of faults in tunnels and its application to TBM jamming analysis. *Tunnelling and Underground Space Technology*, 128, p.104650.

Ye, Z., Xu, Y., Huang, R., Tong, X., and Stilla, U. (2020). Lasdu: a large-scale aerial lidar dataset for semantic labeling in dense urban areas. *International Journal of Geo-Information*, 9(7), 450.

Yi, X., Feng, W., Wang, D., Yang, R., Hu, Y., and Zhou, Y. (2023). An efficient method for extracting and clustering rock mass discontinuities from 3D point clouds. *Acta Geotechnica*, 18(7), 3485-3503.

Zhang, T., Cui L., Zhou L., Liu, J., Kou, L., and Xie Q. (2025). A Roughness, Feature-based Algorithm of Point
Cloud Segmentation of the Secondary Lining in NATM Tunnel. *Acta Polytechnica Hungarica*, 22(4).

Zhao, H., Jiang, L., Fu, C. W., and Jia, J. (2019). PointWeb: Enhancing Local Neighborhood Features for Point Cloud Processing. *2019 IEEE/CVF Conference on Computer Vision and Pattern Recognition (CVPR). IEEE.*

Zhao, Y., Zhu, Z., Liu, W., Zhan, J. and Wu, D., (2023). Application of 3D laser scanning on NATM tunnel deformation measurement during construction. *Acta Geotechnica*, 18(1), pp.483-494.

Zolanvari, S. M. I., Ruano, S., Rana, A., Cummins, A., Da Silva, R. E., and Rahbar, M. (2019). Dublincity: annotated lidar point cloud and its applications.